WILEY

ORIGINAL ARTICLE OPEN ACCESS

Prognostic Significance, Radiological, and Metabolic Characteristics of Metastatic Lymph Nodes in Resectable Non-Small Cell Lung Cancer Following Neoadjuvant Chemoimmunotherapy

Tianxiao Han[1] | Sida Cheng[1] | Xun Wang[1] | QingYi Qi[2] | Jinchuan Chen[3] | Wenxiang Wang[1] | Jian Zhou[1] | Yun Li[1] | Kezhong Chen[1] | Hao Li[1] | Fan Yang[1]

[1]Department of Thoracic Surgery, Thoracic Oncology Institute, Peking University People's Hospital, Beijing, China | [2]Department of Radiology, Peking University People's Hospital, Beijing, China | [3]Department of Nuclear Medicine, Peking University People's Hospital, Beijing, China

Correspondence: Kezhong Chen (chenkezhong@pkuph.edu.cn) | Hao Li (lihao_pkuhsc@163.com) | Fan Yang (yangfan@pkuph.edu.cn)

ABSTRACT

Background: Metastatic lymph nodes (mLNs) exhibit different responses to neoadjuvant immunotherapy compared to the primary tumor (PT) in non-small cell lung cancer (NSCLC). Evaluating mLNs' response is crucial for predicting treatment efficacy and prognosis; however, such assessments are currently insufficient.

Methods: We enrolled 101 NSCLC patients with mLNs who underwent neoadjuvant chemoimmunotherapy followed by surgery. Survival outcomes and radiological and metabolic changes were analyzed across different lymph node pathological response groups, and a least absolute shrinkage and selection operator (LASSO) logistic regression model was developed to predict mLNs' response. RNA sequencing was performed to characterize the immune microenvironment of lymph nodes with different pathological responses.

Results: Residual tumors in mLNs were significantly associated with worse recurrence-free survival ($p = 0.003$) and a trend toward worse overall survival ($p = 0.087$). Combining the pathological responses of mLNs and PTs improved prognostic stratification. Neither radiological size changes (AUC: 0.621) nor the SUVmax reduction rate (AUC: 0.645) were effective in distinguishing mLNs response. A model combining radiological and metabolic parameters demonstrated fair prediction efficacy (AUC: 0.85). In separate analyses of N1 and N2 nodes, radiological and metabolic changes of N1 mLNs partly reflected their pathologic response

----

(AUC: 0.734; 0.816), unlike in N2 mLNs. RNA sequencing revealed that immune infiltration in responding lymph nodes differed from non-responding ones, with higher CD8+ T cells, NK T cells, B cells, and dendritic cells in the former.

Conclusion: The pathological response of mLNs provides additional prognostic information, but current tools are ineffective for detecting residual tumors. A model integrating radiological and metabolic parameters may offer better prediction.

1 | Introduction

The advent of immunotherapy has not only changed the treatment paradigms of advanced non-small cell lung cancer (NSCLC) [1–3] but also deeply revolutionized the perioperative treatment of resectable NSCLC in recent years. Various clinical trials have demonstrated that employing immune checkpoint inhibitors (ICIs) alone or in combination with chemotherapy before surgery can achieve a much higher pathological complete response (pCR) or major pathological response (MPR) rate and significantly improve survival [4–7].

Recently, several real-world studies and clinical practice in our center have found that the metastatic lymph nodes (mLNs) and the paired primary tumor (PT) in the same NSCLC patient may respond differently to ICI treatment (Figure 1A) [8, 9]. Current neoadjuvant studies mainly focused on the assessment and tumor microenvironment (TME) of PT, while the tumor-draining lymph nodes (TDLNs) did not get enough attention.

Reportedly, TDLNs play a fundamental role in anti-tumor immunity and immunotherapy response [10, 11], while their complete resection abrogates the antitumor effect of PD-1/PD-L1 inhibition due to the immune impairment [12, 13]. On the contrary, the mLNs undergo profound structural remodeling and form a suppressive TME that promotes immune suppression

and tolerance for tumor progression [14, 15]. This contradictory but prominent role of TDLNs in tumor immunity makes them indispensable in assessing neoadjuvant treatment efficacy.

Meanwhile, the pathological status of mLNs has been proven to be associated with patient survival in the setting of neoadjuvant immunotherapy [9, 16]. This underscores the importance of independent assessment of mLNs. However, independent evaluation of TDLNs has not yet become a clinical standard, and data on their imaging features before and after immunotherapy remain exceedingly limited [17, 18].

In this study, we assessed the impact of neoadjuvant chemoimmunotherapy on resected mLNs and explored how pathologic response correlates with prognosis. Moreover, we looked into radiological and metabolic changes in mLNs, further distinguishing between N1 and N2 stations. Based on these findings, we developed a model combining radiological and metabolic parameters to predict the pathological status of mLNs. We also investigated distinct immune infiltration between responding mLNs and non-responding ones, aiming to explore the underlying immune microenvironment changes. These results contribute to a deeper understanding of the clinical significance of LN assessment in the context of neoadjuvant immunotherapy, facilitating the prediction of treatment response and development of LN-oriented perioperative treatment strategies.
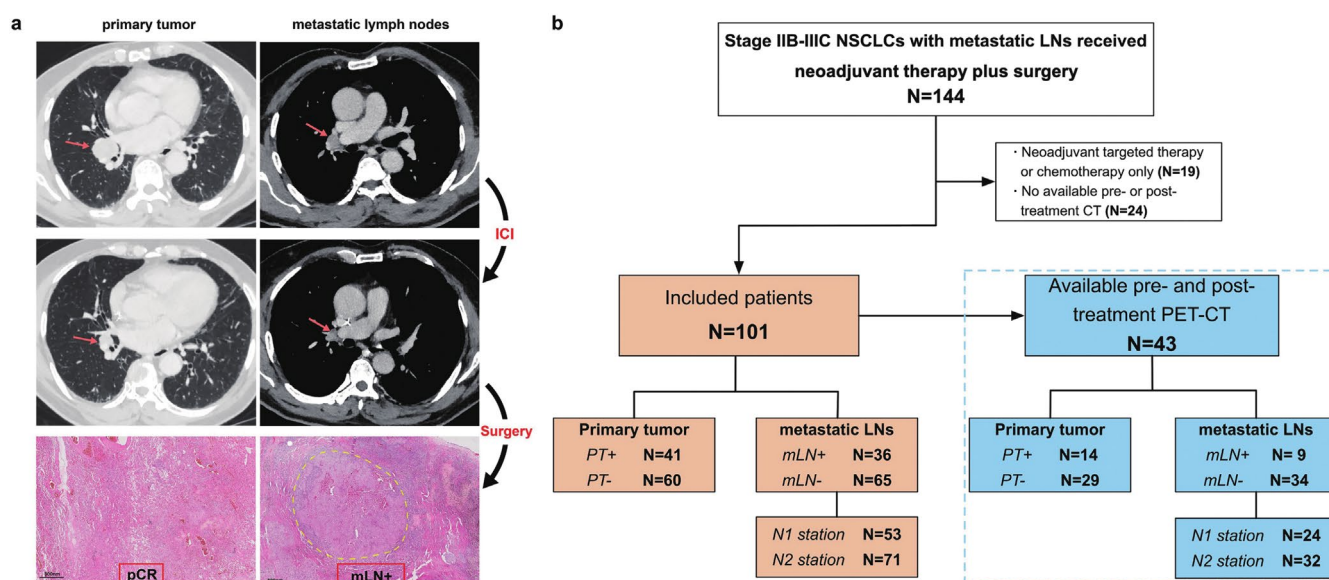
FIGURE 1 | Study design. (A) Response of metastatic lymph nodes (mLNs) to neoadjuvant immunotherapy differs from that of the primary tumor (PT) in clinical practice. Representative images of a non-small cell lung cancer (NSCLC) patient who showed a partial radiological response after neoadjuvant immunotherapy, with a complete pathological response (pCR) in the PT but tumor residuals in the mLN (mLN+). (B) A total of 101 patients with IIB-IIIC NSCLC who received neoadjuvant immunotherapy followed by surgery were included and 43 patients with paired PET/CT were analyzed separately. We divided patients into two groups based on the pathologic status of mLNs: Residual tumor cells (mLN+) and tumor-free (mLN−). Similarly, PTs were divided into PT+ (> 10% residual tumor cells) and PT− (major pathological response). Additionally, N1 and N2 station lymph nodes were analyzed separately.

2 | Methods

2.1 | Study Population and Design

We reviewed the prospectively maintained databases of locally advanced NSCLC patients undergoing neoadjuvant chemoimmunotherapy and subsequent surgery between Jan 2021 and Dec 2023 at Peking University People's Hospital (Figure 1B). Patients with histologically or radiologically confirmed pre-treatment lymph node metastasis were enrolled. All patients received chest computed tomography (CT) or positron emission tomography-computed tomography (PET/CT) scans within 2 weeks prior to the first neoadjuvant cycle to evaluate tumor burden and disease staging accurately. CT or PET/CT scans were repeated 4–6 weeks post the last cycle to assess the therapeutic effect and make a surgical plan. Patients receiving other neoadjuvant therapies, such as target therapy or chemotherapy, without available pre- or post-treatment CT data, or participating in any clinical trial, were excluded.

2.2 | Enrollment of Metastatic Lymph Nodes

Metastatic lymph nodes were identified based on CT imaging features such as enlargement (short-axis diameter ≥ 10 mm), irregular morphology, and significant enhancement. They were confirmed through pathological evidence in most patients or elevated SUVmax on PET/CT scans. For 26 patients with clinical N1 disease, the diameter and SUVmax of the largest N1 lymph node were measured. For 75 patients with clinical N2 disease, the same parameters were measured for the largest N2 lymph node. Among them, 23 patients had concurrent N1 metastasis confirmed by EBUS and evaluable CT or PET/CT data; thus, both their largest N1 and N2 lymph nodes were included.

2.3 | Radiological and Metabolic Assessments

The radiological size was measured in CT or PET/CT scan, defined as the maximum diameter of PT and short-axis diameter of mLNs. Metabolic parameters included the pre-treatment maximum standardized uptake value (SUV_{max}), post-treatment SUVmax, and metabolic reduction rate (ΔSUV_{max}) calculated by the following formula: $\Delta SUV_{max} = $ (pre-treatment SUVmax-post-treatment SUVmax)/pre-treatment SUVmax $\times 100\%$. The therapeutic efficacy was evaluated based on the immune response evaluation criteria in solid tumors (iRECIST) [19].

2.4 | Treatment Overview

Most patients received neoadjuvant chemotherapy combined with 2–4 cycles of PD-1 inhibitors, and a few received one or more than four cycles of treatment. About 4–6 weeks after the final dose, video-assisted thoracoscopic surgery (VATS) or thoracotomy with systemic lymphadenectomy was performed by specialized surgeons using Wang's technique [20]. Standard or extended lobectomies were chosen according to the lesion extent and intraoperative situation. Systemic lymphadenectomy was performed with at least three N1 and three N2 stations. The

clinical and pathologic disease staging was assessed according to the American Joint Committee on Cancer (AJCC) Lung Cancer Staging (8th edition).

2.5 | Pathological Evaluation

The surgical specimens were handled and assessed by two experienced pathologists according to the IASLC neoadjuvant pathology recommendations [21]. Determination of the pathologic response to therapy was made after reviewing all H&E slides of the tumor and lymph nodes by estimating the percentages of viable tumors with 10% increments. The definition of MPR is less than or equal to 10% of viable tumors. No viable tumor cell was classified as pCR. Over 10% of viable tumors were labeled non-pCR/MPR.

2.6 | Feature Selection and Model Construction

We utilized the least absolute shrinkage and selection operator (LASSO) logistic regression analysis for modeling, which shrinks some coefficients of variables to zero using L1 regularization. First, we selected the optimal features using the leave-one-out cross-validation (LOOCV) approach to avoid the randomness of traditional selection methods. Each sample was used as the test set once, while the remaining samples were used for training. This process was repeated for every sample. The frequency of feature appearance was used to measure its significance in the model. We selected the four most important features for further modeling. Next, LASSO logistic regression was applied to build the model, and 3-fold cross-validation was used to select the hyper-parameter λ. The features selected in this process remained consistent with those identified in the LOOCV. Finally, we evaluated the final model performance using the receiver operating characteristic (ROC) curve and the area under the curve (AUC) value.

2.7 | RNA Sequencing

We retrospectively collected available fresh or formalin-fixed paraffin-embedded mLN tissues from 16 enrolled patients for RNA sequencing. The data were normalized and transformed into fragments per kilobase of exon model per million mapped fragments. Then we used the xCell algorithm [22], a novel gene signature-based method to infer 64 immune and stromal cell types in the tumor microenvironment, to quantify the abundance of infiltrating immune cells in our samples.

2.8 | Follow-Up and Outcome

The follow-up information was obtained from postoperative visits, medical records, or telephone calls. Recurrence-free survival (RFS) was defined as the duration from surgery to the last follow-up or the first documented cancer relapse determined by imaging or histopathological evidence. Overall survival (OS) was defined as the duration from surgery to death from any cause or the last follow-up.

2.9 | Statistical Analysis

The Kaplan–Meier survival analysis was used to assess the correlation between pathological status and RFS or OS by Log-rank test. Cox regression analysis was used to adjust for the relevant variables to evaluate the prognostic significance. Continuous variables were presented as median (interquartile range) and compared by Mann–Whitney test or unpaired t-test. Categorical variables were presented as percentages and compared by Chi-square test. The LASSO logistic regression analysis was used to screen among the radiological parameters, subsequently constructing a model to predict the pathological response of lymph nodes. The ROC curve and AUC value were utilized to assess the predictive accuracy. All analyses were performed using R 4.2.1 (R Core Team, Vienna, Austria), GraphPad Prism 9.5.0 (GraphPad Software, San Diego, California, USA), Python 3.12.5 (Python Software Foundation). The two-sided $p < 0.05$ was deemed statistically significant.

3 | Results

3.1 | Study Population

Overall, 101 NSCLC patients with mLNs who received neoadjuvant chemoimmunotherapy and surgery were enrolled, and the data of 124 mLNs were analyzed (Figure 1B). The detailed clinicopathologic characteristics are shown in Table 1. After neoadjuvant therapy, 64 (63.4%) patients achieved partial response, 33 (32.7%) attained stable disease, and 4 (4.0%) had progressive disease according to iRECIST criteria [19]. As for the pathological response, 49 (48.5%) patients achieved MPR, among which 35 (34.7%) patients achieved pCR.

In our cohort, 60 (59.4%) patients achieved MPR in their primary tumors, including 41 (40.6%) with pCR; these patients were designated as the PT− group. The remaining 41 (40.6%) patients exhibited non-pCR/MPR in PTs and were categorized as the PT+ group. Nodal downstaging was observed in 71 (70.3%) patients. In 75 patients with clinical N2 disease, 50 (66.7%) and 6 (8.0%) patients were downstaged to ypN0 and ypN1 after treatment, respectively. Fifteen out of 26 (57.7%) patients with clinical N1 disease were downstaged to ypN0.

Based on postoperative pathological results, patients with complete tumor clearance in mLNs ($n = 65$, 64.4%) were classified as the mLN− group, and those with residual tumors in mLNs ($n = 36$, 35.6%) were classified as the mLN+ group. Compared with the mLN− group, patients in the mLN+ group have significantly more non-squamous NSCLCs ($p < 0.001$), lower downstaging rates ($p < 0.001$), and worse pathological responses of PTs ($p < 0.001$). Interestingly, no significant difference was observed in imaging-related parameters, highlighting the limitations of CT-based response evaluation criteria in the context of immunotherapy.

3.2 | Association Between Pathological Response and Survival

During a median follow-up of 23.7 months (IQR 15.8–32.9), 15 (14.9%) patients died, among which 11 (10.9%) were lung cancer-specific deaths. Twenty-one (20.8%) patients experienced tumor recurrence. Kaplan–Meier analysis demonstrated patients with mLN+ had significantly worse RFS than patients with mLN− ($p = 0.003$), and there was a trend toward a shorter OS ($p = 0.087$) in the mLN+ cases (Figure 2A). The significantly better RFS ($p < 0.001$) and OS ($p < 0.001$) for PT− patients were also observed (Figure 2B). When integrating the assessment of PTs and mLNs, a graduated improvement in RFS ($p = 0.001$) and OS ($p = 0.004$) was observed comparing patients with T−N−, T−N+, T+N− to T+N+, indicating that the pathological node status provides additional prognostic information and contributes to a more accurate risk stratification (Figure 2C). Moreover, patients with postoperative pathological multi-station N2 involvement had significantly worse RFS ($p = 0.029$) and OS ($p = 0.003$) compared to those with single-station N2 metastases, who showed survival outcomes comparable to those with N1 metastases (RFS: $p = 0.630$; OS: $p = 0.657$) (Figure 2D).

Among 21 recurrences, there were 13 local-regional recurrences (LRR) and 8 distant recurrences (DR). One patient with LRR also experienced bilateral lung recurrence. The most common LRR was mediastinal lymph node recurrence (11/13, 84.6%), and the most common location of DR was the brain (6/8, 75.0%) (Table S1). Thirteen (13/36, 36.1%) patients in the mLN+ group experienced recurrence, including 7 cases of LRR and 6 cases of DR. Among the 7 LRR, 5 were lymph node recurrences (5/7, 71.4%), indicating that lymph node recurrence was the main cause of local relapse in the mLN+ group. All 6 cases of distant metastasis occurred in patients with PT+, indicating that more than 10% residual tumor in the primary tumor may lead to a higher risk of distant metastasis. In contrast, only 8 (8/65, 12.3%) patients in the mLN− group experienced tumor recurrence.

Consistently, univariate Cox regression analysis showed that pathological responses of mLNs (multi-station N2 metastases vs. ypN0, HR = 12.410, $p < 0.001$; N1 metastases vs. ypN0, HR = 2.945, $p = 0.06$) and PT (PT+ vs. PT−, HR = 4.780, $p = 0.001$) were significantly associated with RFS (Table 2). In the multivariate analysis, N1 metastases lost their significance, while multi-station N2 metastases and poor PT response remained independent predictors of worse RFS. However, pathological responses of mLNs did not demonstrate independent prognostic value for OS (Table S2). These results reminded us that pathological response in LNs impacts survival outcomes. Lymph node residual disease was associated with increased recurrence risk, and subsequent treatment may play a crucial role in improving prognosis. Therefore, accurately identifying residual lymph nodes preoperatively and strengthening treatment may also be beneficial. Moreover, the surgical approach was associated with RFS ($p = 0.006$) and OS ($p = 0.013$) in univariate analysis. However, thoracotomy lost its significance in multivariate analysis after adjusting for other confounding factors. This may indicate that the surgical approach indirectly reflects the pathological response of the PTs.

3.3 | Radiological and Metabolic Changing Patterns of Metastatic Lymph Nodes

By comparing radiological images before and after treatment, we observed a dramatic size reduction of mLNs, regardless

TABLE 1 | Association between clinicopathologic factors and pathologic response of mLNs.

	Factors	Total (*n* = 101)	mLN+ (*n* = 36)	mLN− (*n* = 65)	*p*
Gender (%)	Male	89 (88.1)	29 (80.6)	60 (92.3)	0.154
	Female	12 (11.9)	7 (19.4)	5 (7.7)	
Age [median (IQR)]		63 (58–68)	64 (58–68)	63 (58–69)	0.755
Smoking history (%)	Never	42 (41.6)	17 (47.2)	25 (38.5)	0.587
	former	25 (24.8)	7 (19.4)	18 (27.7)	
	Current	34 (33.7)	12 (33.3)	22 (33.8)	
Clinical stage (%)	IIb	17 (16.8)	8 (22.2)	9 (13.8)	0.526
	IIIa	54 (53.5)	19 (52.8)	35 (53.8)	
	IIIb	28 (27.7)	9 (25.0)	19 (29.2)	
	IIIc	2 (2.0)	0 (0.0)	2 (3.1)	
Location of primary tumor (%)	Central	34 (33.7)	11 (30.6)	23 (35.4)	0.623
	Peripheral	67 (66.3)	25 (69.4)	42 (64.6)	
Histologic subtype (%)	LUSC	64 (63.4)	15 (41.7)	49 (75.4)	**< 0.001*****
	Non-LUSC	37 (36.6)	21 (58.3)	16 (24.6)	
Cycles of Neoadjuvant therapy (%)	1–2	17 (16.7)	6 (16.7)	11 (16.9)	0.912
	3–4	82 (80.3)	29 (80.6)	53 (81.5)	
	> 4	2 (3.0)	1 (2.8)	1 (1.5)	
Resection type (%)	Pneumonectomy	8 (7.9)	5 (13.9)	3 (4.6)	0.348
	Bilobectomy	8 (7.9)	4 (11.1)	4 (6.2)	
	Sleeve lobectomy	9 (8.9)	2 (5.6)	7 (10.8)	
	Lobectomy	74 (73.3)	24 (66.7)	50 (76.9)	
	Sublobar resection	2 (2.0)	1 (2.8)	1 (1.5)	
Surgical approach (%)	VATS	89 (88.1)	31 (86.1)	58 (89.2)	0.643
	Open	12 (11.9)	5 (13.9)	7 (10.8)	
Surgical margin (%)	R0	99 (98.0)	34 (94.4)	65 (100.0)	0.240
	R1	2 (2.0)	2 (5.6)	0 (0.0)	
Duration from final dose to surgery, days		37 (29–48)	38 (28–52)	35 (30–44)	0.796
Pre-treatment PT diameter, cm [median (IQR)]		4.3 (3.3–5.9)	4.2 (3.2–5.4)	4.5 (3.3–6.3)	0.650
Post-treatment PT diameter, cm [median (IQR)]		2.8 (1.7–3.9)	2.9 (1.8–3.8)	2.7 (1.6–4.0)	0.450
Pre-treatment mLNs diameter, cm [median (IQR)]		1.4 (1.1–1.7)	1.3 (1.1–1.7)	1.4 (1.1–1.7)	0.898
Post-treatment mLNs diameter, cm [median (IQR)]		1.0 (0.7–1.2)	1.1 (0.8–1.2)	0.9 (0.7–1.2)	0.263
No. of resected LN stations [median (IQR)]		7.0 (6.0–7.0)	6.5 (6.0–7.0)	7.0 (6.0–7.0)	0.558
No. of resected LNs [median (IQR)]		12.0 (9.5–17.5)	13.5 (9.3–16.8)	12.0 (9.5–18.0)	0.969

(Continues)

TABLE 1 | (Continued)

	Factors	Total ($n = 101$)	mLN+ ($n = 36$)	mLN− ($n = 65$)	p
Radiologic Response (%)	PR	64 (63.4)	22 (61.1)	42 (64.6)	0.814
	SD	33 (32.7)	12 (33.3)	21 (32.3)	
	PD	4 (4.0)	2 (5.6)	2 (3.1)	
Pathological Response of PT (%)	pCR	41 (40.6)	6 (16.7)	35 (53.8)	**< 0.001*****
	MPR	19 (18.8)	5 (13.9)	14 (21.5)	
	Non-pCR/MPR	41 (40.6)	25 (69.4)	16 (24.6)	
Pathologic downstaging (%)	Yes	77 (76.2)	13 (36.1)	64 (98.5)	**< 0.001*****
	No	24 (23.8)	23 (63.9)	1 (1.5)	
Nodal downstaging (%)	Yes	71 (70.3)	6 (16.7)	65 (100.0)	**< 0.001*****
	No	30 (29.7)	30 (83.3)	0 (0.0)	

*Note: *, **, ***, statistically significant difference.*

Abbreviations: LUSC, lung squamous cell carcinoma; mLN+, tumor residuals in mLN; mLN−, complete tumor clearance in mLN; mLNs, metastasis lymph nodes; MPR, pathological major response; pCR, pathological complete response; PD, progressive disease; PR, partial response; PT, primary tumor; R0, radical resection; R1, microscopically positive resection margin; SD, stable disease; VATS, video-assisted thoracoscopic surgery.

of the pathological nodal status (Figure 3A). Although the size reduction was more obvious in the mLN− group, the low AUC value of 0.621 suggested that the efficacy of radiological changes to discriminate the pathological response of mLNs was not good enough. The changes in PTs size did not significantly differ between the mLN+ and mLN− groups (Figure 3B). In the separate analysis of 53 involved N1 and 71 N2 mLNs, we found that the reduction rate of N1 size was significantly higher in the mLN− group compared with the mLN+ group, rather than N2 nodes (Figure 3C,D). The ROC curve proved that the radiological changes in N1 nodes demonstrated a better predictive ability for the pathologic response degree (AUC: 0.734) than those in N2 nodes (AUC: 0.522). This brings us to an important point that evaluating the different node stations separately is important in the neoadjuvant ICI treatment setting for NSCLC.

Then, we analyzed the metabolic changing patterns of 56 mLNs in 43 patients with paired pre- and post-treatment PET/CT. Their baseline characteristics were summarized in Table S3. We observed a significant reduction in SUV_{max} of lymph nodes within the mLN− group ($p < 0.001$), whereas the mLN+ group did not exhibit a similar trend ($p = 0.159$). However, the $\triangle SUV_{max}$ of lymph nodes between these two groups was not statistically significant ($p = 0.157$), indicating that metabolic changes have limited ability to distinguish pathological responses in mLNs (AUC: 0.645) (Figure 4A). As for PTs, we found a significant decline of SUVmax in all groups, even in the mLN+ ($p = 0.004$) group (Figure 4B). Although the $\triangle$SUVmax of the PTs was notably higher in the mLN− group ($p = 0.019$), this difference was insufficient to clearly distinguish between different lymph node response groups (AUC: 0.717). Metabolic changing patterns of 24 N1 mLNs and 32 N2 mLNs were further compared. The $\triangle SUV_{max}$ of N1 nodes proved to be a fair indicator of the pathologic nodal status (AUC: 0.816), and the optimal cut-off value was 55.3% to distinguish mLN− from mLN+. Conversely, the $\triangle SUV_{max}$ of N2 nodes displayed no predictive value (AUC: 0.504) (Figure 4C,D). Additionally, metabolic changes of mLNs

and PTs were irrespective of the pathological responses in primary tumor beds (Figure S1).

3.4 | The Prediction Model for the Pathological Status of Metastatic Lymph Nodes

Given that the single radiological or metabolic parameter was not effective in predicting the pathologic responses of mLNs, we attempted to construct a combined model to achieve more accurate predictions. The LASSO regression model was used to filtrate the radiological and metabolic parameters related to the pathological nodal status. We chose λ with the minimum cross-entropy error (λ = 1.6448), and post-treatment PT size, size reduction rate of PT, ΔSUVmax of PT, and ΔSUVmax of mLNs were selected after LOOCV and regression analyses (Figure 5A–C). The model formula is as follows: 0.18 × post-treatment PT size—0.31 × diameter reduction rate of PT—1.73 × ΔSUVmax of PT—0.51 × ΔSUVmax of mLNs—0.19. The model showed good predictive performance for residual tumors in lymph nodes with an AUC value of 0.85%, 76.0% specificity, and 83.3% sensitivity via the ROC curve (Figure 5D). We preliminarily validated the model in a cohort of 19 NSCLC patients with lymph node metastasis and paired PET/CT data who underwent neoadjuvant chemoimmunotherapy and surgery at our center between January and September 2024. The model demonstrated an AUC of 0.76 (95% CI: 0.53–0.99), indicating reasonable performance (Figure S2).

3.5 | Immune Infiltration Heterogeneity and Its Correlation With Pathological Responses

The surgical samples of mLNs from 16 patients were collected, and the expression profiling was performed by high-throughput bulk RNA sequencing (Figure S3). For the first time, we tried to compare the immune infiltration status between mLNs with different pathological responses. The density of CD8^{+} T cells, B cells, NKT cells, and dendritic cells (DCs) was significantly higher in
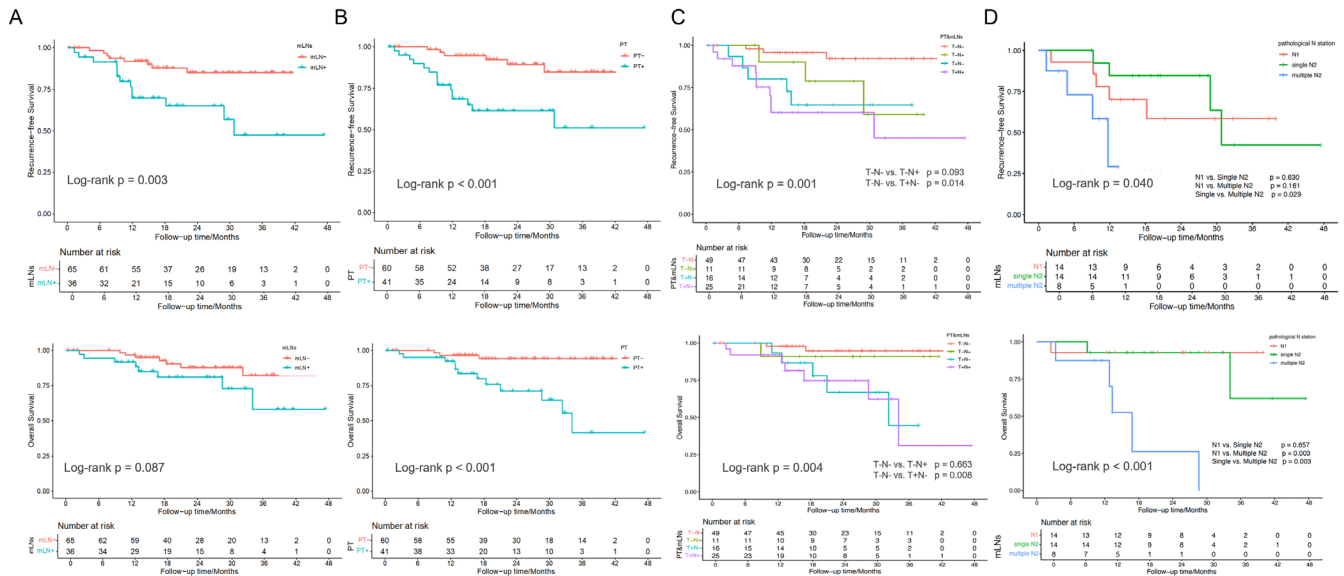
FIGURE 2 | Kaplan–Meier curves on patient survival by pathologic status. Recurrence free survival (RFS; upper row) and overall survival (OS; lower row) of patients receiving neoadjuvant immunotherapy in the mLN+/mLN− subgroups (A), in the PT+/PT− subgroups (B), and in the T−N−/T−N+/T+N−/T+N+ subgroups (C). Of these, mLN+ represents residual tumor cells in mLNs and mLN− represents complete tumor clearance in mLNs. PT+ indicates more than 10% residual tumor cells in PT and PT− indicates major pathological response in PT. T−N−/T−N+/T+N−/T+N+ represent combinations of mLN+/mLN− and PT+/PT−. (D) RFS (upper) and OS (lower) by pathological N stages among mLN+ patients, including N1 involvement, single-station N2 involvement and multi-station N2 involvement. The *p*-value was calculated by the log-rank test. Vertical tick marks represent censored subjects.

TABLE 2 | Univariate and multivariate cox analysis of factors associated with RFS.

Variable	Univariate analysis			Multivariate analysis		
	HR	95% CI	*p*	HR	95% CI	*p*
Sex (male vs. female)[a]	/	/	/			
Age (> 65 vs. ≤ 65)	0.538	0.171–1.698	0.29			
Smoking (ever vs. never)	1.122	0.447–2.820	0.81			
Clinical stage (IIIB-IIIC vs. II-IIIA)	1.309	0.525–3.270	0.56			
Preoperative PT size (> 4 cm vs. ≤ 4 cm)	2.302	0.924–5.732	**0.07**	1.901	0.623–5.795	0.26
Centrally located tumor (central vs. peri)	0.921	0.371–2.290	0.86			
Histology (LUSC vs. non-LUSC)	1.729	0.633–4.730	0.29			
Resection type (extended vs. standard lobectomy)	1.853	0.766–4.480	0.17	1.836	0.254–13.264	0.55
Surgical approach (Open vs. VATS)	3.797	1.474–9.809	**0.006**	3.407	0.977–11.878	0.06
Surgical margin (R1 vs. R0)[a]	/	/	/			
Radiological response (SD + PD vs. PR)	1.211	0.501–2.929	0.67			
Pathological response of PT (non-pCR/MPR vs. pCR/MPR)	4.780	1.847–12.37	**0.001**	3.196	1.040–9.819	**0.04**
Pathological N staging[b]						
ypN1 vs. ypN0	2.945	0.962–9.013	**0.06**	2.371	0.710–7.923	0.16
ypN2a vs. ypN0	2.447	0.736–8.131	0.14	1.426	0.311–6.529	0.65
ypN2b vs. ypN0	12.410	3.411–45.148	**< 0.001**	4.974	1.121–22.077	**0.03**

Note: Statistically significant difference is shown in bold.

Abbreviations: LUSC, lung squamous cell carcinoma; MPR, major pathological response; pCR, pathological complete response; PD, progression disease; PR, partial remission; PT, primary tumor; RFS, recurrence-free survival; SD, stable disease; VATS, video-assisted thoracic surgery.

[a]All 21 cases of recurrence occurred in male patients and were R0 resection.

[b]Based on the 9th edition of TNM: ypN2a (single-station N2 involvement), ypN2b (multi-station N2 involvement).
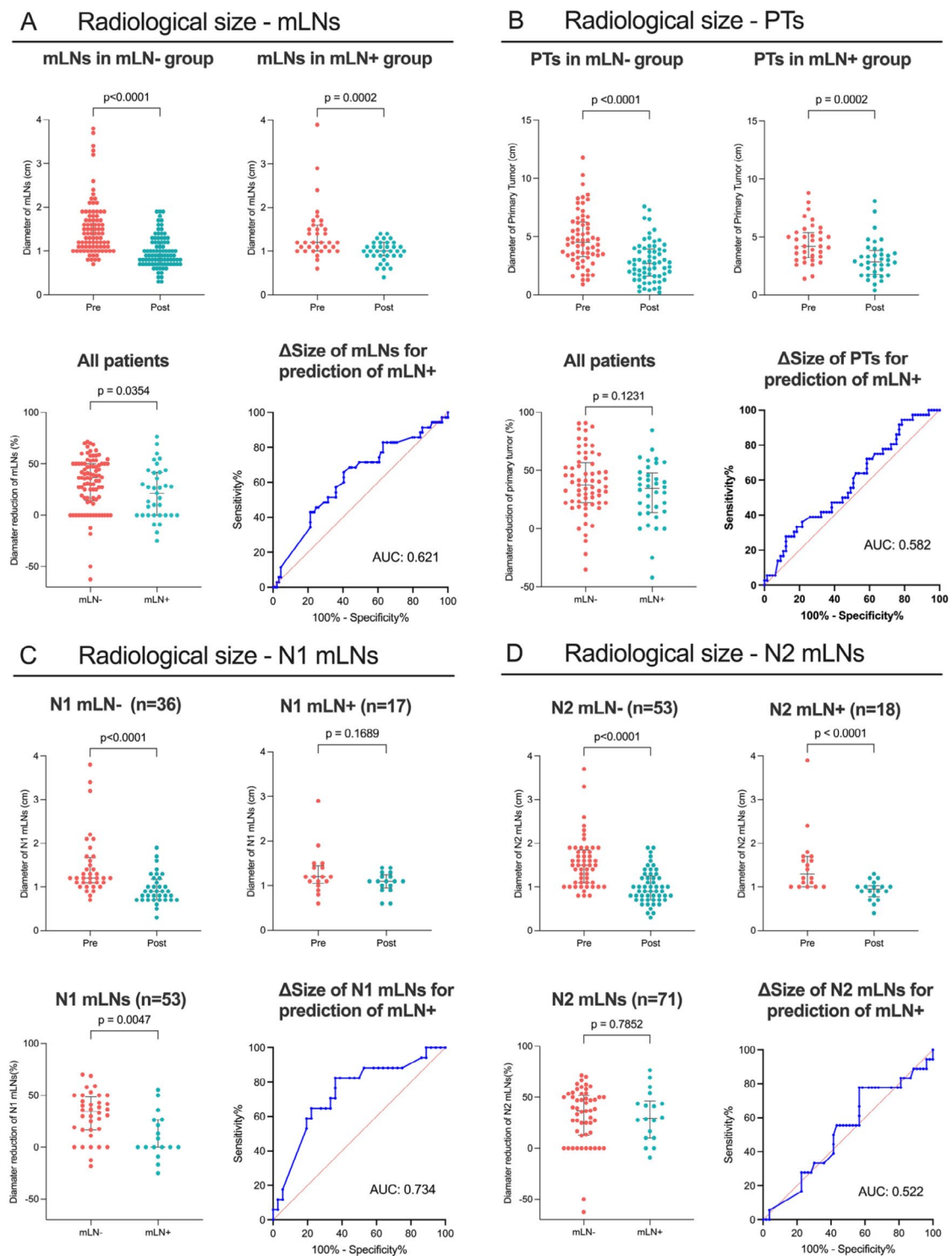
FIGURE 3 | Radiological changing patterns of metastatic lymph nodes (mLNs), primary tumors (PTs), and N1/N2 lymph nodes. The radiological changes of (A) mLNs and (B) PTs, (C) N1 station mLNs and (D) N2 station mLNs in mLN−/mLN+ subgroups and their predictive value for pathological response of mLNs. Of these, mLN+ represents residual tumor cells in mLNs and mLN− represents complete tumor clearance in mLNs. The p-value was calculated using an unpaired two-sided t-test for normally distributed data or the Mann–Whitney U test. Receiver operating characteristic (ROC) curve analysis was used to assess the predictive accuracy in predicting pathologic responses of mLNs.

the mLN− group compared to the mLN+ group, indicating their positive roles in therapeutic response, while smooth muscle cells with restraining function were more abundant in the poor efficacy group (Figure S3). We further investigated the association between immune infiltration status and survival outcomes, but found no statistically significant differences (Figure S4).
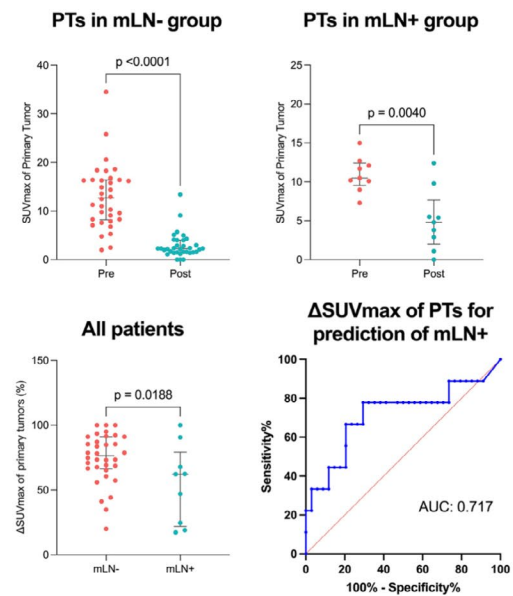
4 | Discussion

Although neoadjuvant ICI therapy has remarkably optimized the treatment paradigms for resectable NSCLC [23], there are still many unresponsive patients. Based on the report that mLNs and PTs can have quite different treatment responses
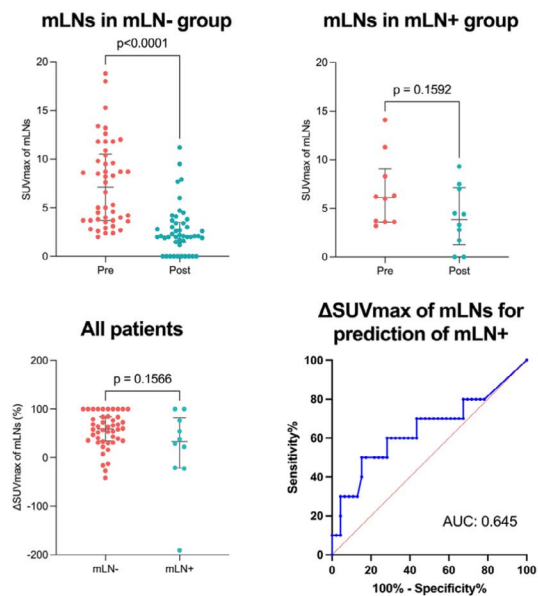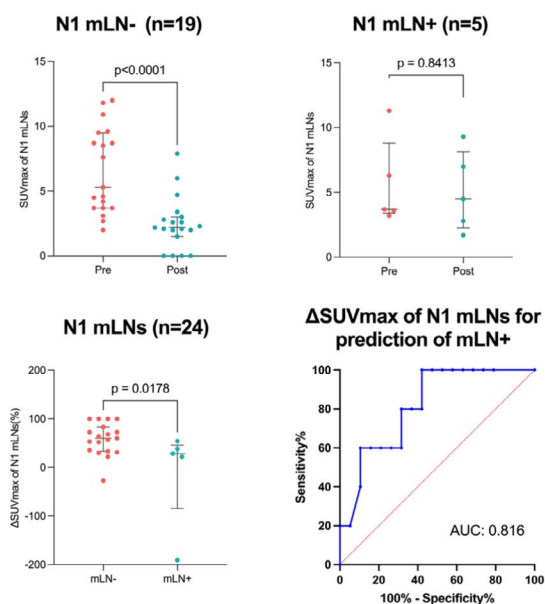
FIGURE 4 | Legend on next page.
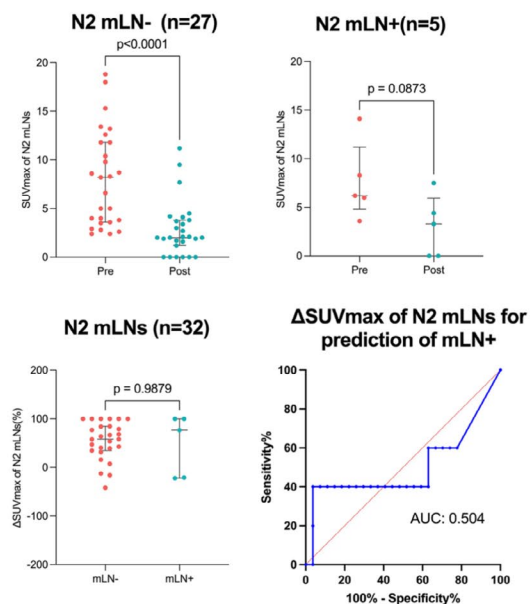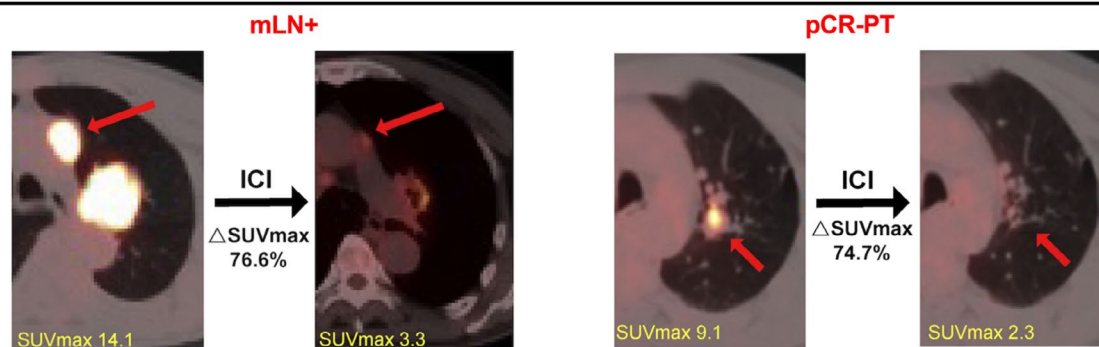
FIGURE 4 | Metabolic changing patterns of metastatic lymph nodes (mLNs), primary tumors (PTs), and N1/N2 lymph nodes. The SUVmax changes on ^{18}F-FDG PET-CT of (A) mLNs and (B) PTs, (C) N1 station mLNs and (D) N2 station mLNs in mLN−/mLN+ subgroups and their predictive value for pathological response of mLNs. (E) A representative case with remarkable reduced SUVmax values achieved pCR in PT and still had tumor residuals in mLN. The *p*-value was calculated using an unpaired two-sided *t*-test for normally distributed data or the Mann–Whitney *U* test. Receiver operating characteristic (ROC) curve analysis was used to assess the predictive accuracy in predicting pathologic responses of mLNs.
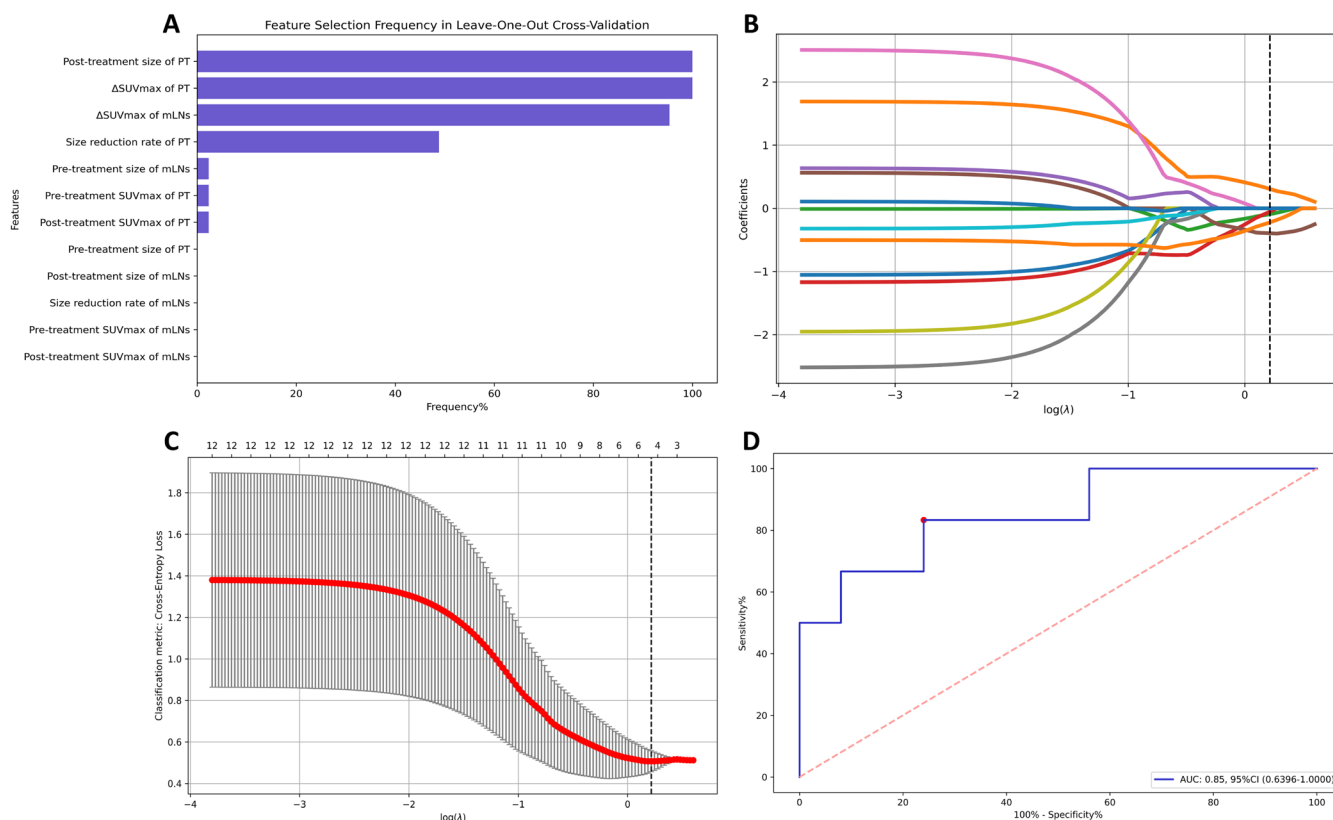
FIGURE 5 | LASSO logistic regression analysis was used to select radiological and metabolic features and establish the final model to predict tumor residuals in mLNs. (A) Feature selection in leave-one-out cross-validation (LOOCV). The blue bars depict the importance of each feature by frequency of appearance. (B) LASSO coefficient profiles of the 12 risk factors. Each curve in the figure presents the change of each variable in coefficient. The vertical dotted line is drawn at the minimum cross-entropy loss ($\lambda = 1.6448$). (C) Three-fold cross-validation was used and the optimal lambda produced five nonzero coefficients (one was smaller than 0.01 and excluded from the final model). The selected four feature are consistent with the most important four using LOOCV in (A). (D) The prediction performance of LASSO logistic regression model by receiver operating characteristic (ROC) curve and the area under the curve (AUC) value.

[4, 8], it is imperative to assess them separately in the context of neoadjuvant ICI treatment. In this real-world study, we comprehensively characterized the association between the therapeutic response of mLNs with imaging features and survival outcomes. Our findings indicate that the pathological status of mLNs had significant impacts on survival and provides additional prognostic information. While size and metabolic changes were insufficient to discriminate pathological responses of mLNs, an integrated predictive model exhibited better efficacy. We also conducted an in-depth analysis of different imaging changes between N1 and N2 stations. Additionally, we observed distinct immune infiltration across mLNs with different pathological responses.

Consistent with previous small-scale research, we demonstrated that tumor clearance in both mLNs and PT is associated with survival in the neoadjuvant scenario [7, 9, 24]. The combination

of them contributed to a more precise outcome stratification, indicating that pathological assessment of mLNs provides additional prognostic information beyond the PT alone. Also, the data from the Checkmate 816 cohort suggested that combining pathologic responses from PT and LNs helped differentiate outcomes [25]. However, we think such prognostic value should not be overstated. We found that there was a similar OS improvement in patients with or without tumor residuals in mLNs when PTs were tumor-free. Inversely, the outcomes of patients in the mLN− group were mainly dependent on the pathological status of PT. This reminded us that patients with tumor residuals only in mLNs, categorized as IIB (ypT0N1) or IIIA (ypT0N2) [26], may have promising survival outcomes with appropriate treatment after surgery. We also found that patients with pathological multi-station N2 lymph node metastasis have significantly worse prognosis under the context of neoadjuvant immunotherapy, which is consistent with the 9th edition TNM staging [27].

The optimal clinicopathological staging system and adjuvant treatment strategies of the NSCLC patients after neoadjuvant ICI treatment still need further exploration.

Additionally, we observed that thoracotomy appeared to have a negative impact on prognosis in the univariate analysis. Compared to VATS, thoracotomy is typically associated with larger tumor size, expanded resection, and centrally located tumors. In our cohort, patients receiving thoracotomy were more likely to have centrally located tumors (58.3% vs. 30.3%, $p = 0.054$) and mostly underwent expanded lobectomy (75% vs. 18%, $p < 0.001$) compared to those receiving VATS. The underlying reasons include high tumor burden, proximity to central vascular and bronchial structures, and extensive invasion. The loss of significance for thoracotomy in multivariate analysis after adjusting for these confounding factors may indicate that the surgical approach indirectly reflects the pathological response of the PTs.

The RECIST, based on CT imaging, has long been regarded as the standard tool to evaluate the treatment response of solid tumors including NSCLCs [19, 28]. However, recent trials and real-world studies on neoadjuvant ICI treatment have demonstrated a poor correlation between radiological changes and pathological responses of PT [4, 6, 29]. Meanwhile, the conventional criteria did not include separate assessments of mLNs aside from PT, and studies investigating mLNs' radiological features are extremely lacking. Yang et al. [18] found that ICI treatment induced a size enlargement of mLNs, which mainly occurred in patients with pCR/MPR in PT. Differently, in our cohort, the radiological size of mLNs was significantly reduced across all subgroups regardless of the pathological response, illustrating an unsatisfying performance of CT for therapeutic assessment. Therefore, the current iRECIST criteria have been challenged, and more precise tools are urgently needed.

PET/CT can reflect tumor metabolic activity, making it a valuable tool for assessing treatment response [30, 31]. Some trials in resectable NSCLCs employing neoadjuvant chemoimmunotherapy reported that SUVmax reduction has a significant correlation with pathologic response and can predict MPR in PTs [32, 33]. However, the systematic analysis of metabolic features of mLNs in the setting of immunotherapy is still rare. Zhang et al. [17] found PET/CT an accurate tool to predict tumor residual in N2 station after neoadjuvant chemoimmunotherapy with an AUC of 0.807 in 86 patients. Yang et al. [18] collected matched pre- and post-treatment data in 12 patients, and a dramatic decrease of mLNs' SUVmax was only observed in the mLN− subgroup. In our study, SUVmax was reduced in the mLN− group compared to the mLN+ group, but there was no significant difference in the △SUVmax between these two groups. These findings suggest that metabolic changes are not a reliable indicator of residual tumors in metastatic lymph nodes (mLNs). However, we found that the combination of radiological and metabolic features of the PTs and metastatic lymph nodes could be an effective method to reflect the pathological response of mLNs. Nevertheless, further validation with a larger sample size is needed in the future. Liquid biopsy or other advanced techniques still need further exploration.

For the first time, we tried to investigate the radiological and metabolic changing patterns of N1 and N2 mLNs based on their

pathological response. The results implied that radiological size changes and especially the SUVmax changes of N1 LNs may help differentiate their pathological status, but not for N2 nodes. Meanwhile, previous reports have found that different LN stations might have heterogeneous treatment responses, making it important to evaluate them separately. In a phase Ib study of neoadjuvant Sintilimab therapy, a higher pCR rate in N1 LNs (6/19, 32%) compared to N2 nodes (1/7, 14%) was observed due to the immune-inflamed microenvironment [8]. We speculate that the therapeutic response of N1 and N2 cannot be generalized, and the immune microenvironment might be the underlying determining factor. Further validations with larger sample sizes and molecular research methods are needed.

However, many patients are still unresponsive to immunotherapy because of tumor heterogeneity or immune resistance [34, 35]. Research suggests that immunotherapy failure or resistance may be closely linked to the immunosuppressive environment within lymph nodes [36]. A comprehensive study of pathological responses and the immune microenvironment could offer valuable insights into the underlying mechanisms, ultimately improving treatment outcomes. We performed RNA sequencing on a few available samples to make a preliminary exploration. The CD8+ T cells, B cells, DCs, and NKT cells seem to play important roles in assisting ICI response. In the mLNs without tumor residual after treatment, the highly infiltrated adaptive and innate immune cells could help promote the effect of subsequent immunotherapy, which is one of the reasons we can consider selectively preserving them during surgery. This is in agreement with prior studies [37] proposed a precise rather than excessive LN dissection strategy to ensure clearance of all metastatic LNs and simultaneously preserve immune-dependent LNs, which will be conducive to better immunotherapy efficacy.

Our study has several limitations. This is a single-center retrospective study, and the selection bias remained inevitable. The follow-up time was relatively short, and the prognostic value needs to be interpreted with caution. A multi-center prospective study with a larger sample size and longer follow-up is further needed. The pathological prediction model of mLNs was established from a small cohort, and validation should be accomplished with a larger sample size. The bulk RNA sequencing was only carried out in a few patients and may not fully represent the immune status of all samples; thus, the results need verification by more sequencing data or immunohistochemical staining.

5 | Conclusions

In summary, we evaluated the impact of mLNs' pathological responses on prognosis and explored radiological and metabolic changes following neoadjuvant chemoimmunotherapy to predict them. Our study demonstrated that the pathological response of mLNs is a crucial prognostic factor and enhances prognostic stratification. However, existing tools are insufficient for accurately predicting pathological responses, particularly in N2 nodes. The model incorporating radiological and metabolic parameters achieved better prediction. Our findings provided further evidence of the clinical significance of lymph node assessment in resectable NSCLC patients undergoing neoadjuvant chemoimmunotherapy. Development of novel preoperative or

intraoperative evaluation tools, modified staging systems, and precise dissection strategies with modified adjuvant treatment for mLNs is essential to improve survival outcomes.

Ethics Statement

This study was approved by the Ethics Committee Board of Peking University People's Hospital (2021PHB271-001, 2022PHB370-001). All patients were informed of the establishment and utilization of the institute database and tissue bank, and written consent was prospectively obtained.

Conflicts of Interest

The authors declare no conflicts of interest.

Data Availability Statement

The data that support the findings of this study are available from the corresponding author upon reasonable request.

References

1. R. S. Herbst, P. Baas, D. W. Kim, et al., "Pembrolizumab Versus Docetaxel for Previously Treated, PD-L1-Positive, Advanced Non-small-Cell Lung Cancer (KEYNOTE-010): A Randomised Controlled Trial," *Lancet* 387, no. 10027 (2016): 1540–1550.

2. M. Reck, D. Rodriguez-Abreu, A. G. Robinson, et al., "Pembrolizumab Versus Chemotherapy for PD-L1-Positive Non-Small-Cell Lung Cancer," *New England Journal of Medicine* 375, no. 19 (2016): 1823–1833.

3. A. Rittmeyer, F. Barlesi, D. Waterkamp, et al., "Atezolizumab Versus Docetaxel in Patients With Previously Treated Non-small-Cell Lung Cancer (OAK): A Phase 3, Open-Label, Multicentre Randomised Controlled Trial," *Lancet* 389, no. 10066 (2017): 255–265.

4. S. Gao, N. Li, S. Gao, et al., "Neoadjuvant PD-1 Inhibitor (Sintilimab) in NSCLC," *Journal of Thoracic Oncology* 15, no. 5 (2020): 816–826.

5. J. E. Chaft, F. Oezkan, M. G. Kris, et al., "Neoadjuvant Atezolizumab for Resectable Non-small Cell Lung Cancer: An Open-Label, Single-Arm Phase II Trial," *Nature Medicine* 28, no. 10 (2022): 2155–2161.

6. M. Provencio, E. Nadal, A. Insa, et al., "Neoadjuvant Chemotherapy and Nivolumab in Resectable Non-small-Cell Lung Cancer (NADIM): An Open-Label, Multicentre, Single-Arm, Phase 2 Trial," *Lancet Oncology* 21, no. 11 (2020): 1413–1422.

7. P. M. Forde, J. Spicer, S. Lu, et al., "Neoadjuvant Nivolumab Plus Chemotherapy in Resectable Lung Cancer," *New England Journal of Medicine* 386, no. 21 (2022): 1973–1985.

8. Y. Ling, N. Li, L. Li, et al., "Different Pathologic Responses to Neoadjuvant Anti-PD-1 in Primary Squamous Lung Cancer and Regional Lymph Nodes," *NPJ Precision Oncology* 4, no. 1 (2020): 32.

9. H. Deng, S. Xiong, R. Zhong, et al., ""Major Pathologic Response" in Lymph Nodes: A Modified Nodal Classification for Non-small Cell Lung Cancer Patients Treated With Neoadjuvant Immunochemotherapy," *Experimental Hematology & Oncology* 12, no. 1 (2023): 40.

10. F. Dammeijer, M. van Gulijk, E. E. Mulder, et al., "The PD-1/PD-L1-Checkpoint Restrains T Cell Immunity in Tumor-Draining Lymph Nodes," *Cancer Cell* 38, no. 5 (2020): 685–700.e8.

11. E. F. Goode, E. T. Roussos Torres, and S. Irshad, "Lymph Node Immune Profiles as Predictive Biomarkers for Immune Checkpoint Inhibitor Response," *Frontiers in Molecular Biosciences* 8 (2021): 674558.

12. M. F. Fransen, M. Schoonderwoerd, P. Knopf, et al., "Tumor-Draining Lymph Nodes Are Pivotal in PD-1/PD-L1 Checkpoint Therapy," *JCI Insight* 3, no. 23 (2018): e124507, https://doi.org/10.1172/jci.insight.124507.

13. V. S. Fear, C. A. Forbes, S. A. Neeve, et al., "Tumour Draining Lymph Node-Generated CD8 T Cells Play a Role in Controlling Lung Metastases After a Primary Tumour Is Removed but Not When Adjuvant Immunotherapy Is Used," *Cancer Immunology, Immunotherapy* 70, no. 11 (2021): 3249–3258.

14. H. du Bois, T. A. Heim, and A. W. Lund, "Tumor-Draining Lymph Nodes: At the Crossroads of Metastasis and Immunity," *Science Immunology* 6, no. 63 (2021): eabg3551.

15. L. Gillot, L. Baudin, L. Rouaud, F. Kridelka, and A. Noel, "The Pre-Metastatic Niche in Lymph Nodes: Formation and Characteristics," *Cellular and Molecular Life Sciences* 78, no. 16 (2021): 5987–6002.

16. X. Liu, W. Sun, J. Wu, et al., "Major Pathologic Response Assessment and Clinical Significance of Metastatic Lymph Nodes After Neoadjuvant Therapy for Non-small Cell Lung Cancer," *Modern Pathology* 34, no. 11 (2021): 1990–1998.

17. L. Zhang, E. Haoran, J. Huang, et al., "Clinical Utility of [(18)F]FDG PET/CT in the Assessment of Mediastinal Lymph Node Disease After Neoadjuvant Chemoimmunotherapy for Non-small Cell Lung Cancer," *European Radiology* 33, no. 12 (2023): 8564–8572.

18. H. Yang, B. Sun, W. Ma, et al., "Multi-Scale Characterization of Tumor-Draining Lymph Nodes in Resectable Lung Cancer Treated With Neoadjuvant Immune Checkpoint Inhibitors," *eBioMedicine* 84 (2022): 104265.

19. L. Seymour, J. Bogaerts, A. Perrone, et al., "iRECIST: Guidelines for Response Criteria for Use in Trials Testing Immunotherapeutics," *Lancet Oncology* 18, no. 3 (2017): e143–e152, https://doi.org/10.1016/S1470-2045(17)30074-8.

20. R. Sullivan, O. I. Alatise, B. O. Anderson, et al., "Global Cancer Surgery: Delivering Safe, Affordable, and Timely Cancer Surgery," *Lancet Oncology* 16, no. 11 (2015): 1193–1224.

21. W. D. Travis, S. Dacic, I. Wistuba, et al., "IASLC Multidisciplinary Recommendations for Pathologic Assessment of Lung Cancer Resection Specimens After Neoadjuvant Therapy," *Journal of Thoracic Oncology* 15, no. 5 (2020): 709–740.

22. D. Aran, Z. Hu, and A. J. Butte, "xCell: Digitally Portraying the Tissue Cellular Heterogeneity Landscape," *Genome Biology* 18, no. 1 (2017): 220.

23. S. P. L. Saw, B. H. Ong, K. L. M. Chua, A. Takano, and D. S. W. Tan, "Revisiting Neoadjuvant Therapy in Non-small-Cell Lung Cancer," *Lancet Oncology* 22, no. 11 (2021): e501–e516, https://doi.org/10.1016/S1470-2045(21)00383-1.

24. A. Pataer, A. Weissferdt, A. A. Vaporciyan, et al., "Evaluation of Pathologic Response in Lymph Nodes of Patients With Lung Cancer Receiving Neoadjuvant Chemotherapy," *Journal of Thoracic Oncology* 16, no. 8 (2021): 1289–1297.

25. J. S. Deutsch, A. Cimino-Mathews, E. Thompson, et al., "Association Between Pathologic Response and Survival After Neoadjuvant Therapy in Lung Cancer," *Nature Medicine* 30, no. 1 (2024): 218–228.

26. D. R. Byrd, J. D. Brierley, T. P. Baker, D. C. Sullivan, and D. M. Gress, "Current and Future Cancer Staging After Neoadjuvant Treatment for Solid Tumors," *CA: A Cancer Journal for Clinicians* 71, no. 2 (2021): 140–148.

27. R. Rami-Porta, K. K. Nishimura, D. J. Giroux, et al., "The International Association for the Study of Lung Cancer Lung Cancer Staging Project: Proposals for Revision of the TNM Stage Groups in the Forthcoming (Ninth) Edition of the TNM Classification for Lung Cancer," *Journal of Thoracic Oncology* 19, no. 7 (2024): 1007–1027.

28. E. A. Eisenhauer, P. Therasse, J. Bogaerts, et al., "New Response Evaluation Criteria in Solid Tumours: Revised RECIST Guideline (Version 1.1)," *European Journal of Cancer* 45, no. 2 (2009): 228–247.

29. Z. R. Zhao, C. P. Yang, S. Chen, et al., "Phase 2 Trial of Neoadjuvant Toripalimab With Chemotherapy for Resectable Stage III Non-small-Cell Lung Cancer," *Oncoimmunology* 10, no. 1 (2021): 1996000.

30. K. Kaira, T. Higuchi, I. Naruse, et al., "Metabolic Activity by (18)F-FDG-PET/CT Is Predictive of Early Response After Nivolumab in Previously Treated NSCLC," *European Journal of Nuclear Medicine and Molecular Imaging* 45, no. 1 (2018): 56–66.

31. D. R. Spigel, J. E. Chaft, S. Gettinger, et al., "FIR: Efficacy, Safety, and Biomarker Analysis of a Phase II Open-Label Study of Atezolizumab in PD-L1-Selected Patients With NSCLC," *Journal of Thoracic Oncology* 13, no. 11 (2018): 1733–1742.

32. Y. Cheng, Z. Y. Chen, J. J. Huang, and D. Shao, "Efficacy Evaluation of Neoadjuvant Immunotherapy Plus Chemotherapy for Non-small-Cell Lung Cancer: Comparison of PET/CT With Postoperative Pathology," *European Radiology* 33, no. 10 (2023): 6625–6635.

33. F. Zhuang, E. Haoran, J. Huang, et al., "Utility of (18)F-FDG PET/CT Uptake Values in Predicting Response to Neoadjuvant Chemoimmunotherapy in Resectable Non-small Cell Lung Cancer," *Lung Cancer* 178 (2023): 20–27.

34. D. Frisone, A. Friedlaender, A. Addeo, and P. Tsantoulis, "The Landscape of Immunotherapy Resistance in NSCLC," *Frontiers in Oncology* 12 (2022): 817548.

35. E. G. Dunne, C. N. Fick, J. M. Isbell, et al., "The Emerging Role of Immunotherapy in Resectable Non-Small Cell Lung Cancer," *Annals of Thoracic Surgery* 118, no. 1 (2024): 119–129.

36. A. J. Schoenfeld, S. J. Antonia, M. M. Awad, et al., "Clinical Definition of Acquired Resistance to Immunotherapy in Patients With Metastatic Non-small-Cell Lung Cancer," *Annals of Oncology* 32, no. 12 (2021): 1597–1607.

37. H. Deng, J. Zhou, H. Chen, et al., "Impact of Lymphadenectomy Extent on Immunotherapy Efficacy in Post-Resectional Recurred Non-small Cell Lung Cancer: A Multi-Institutional Retrospective Cohort Study," *International Journal of Surgery* 110, no. 1 (2023): 238–252, https://doi.org/10.1097/JS9.0000000000000774.

Supporting Information

Additional supporting information can be found online in the Supporting Information section.